Available online at www.sciencedirect.com
SCIENCE DIRECT®
ELSEVIER
International Journal of Impact Engineering 31 (2005) 699–717
INTERNATIONAL JOURNAL OF IMPACT ENGINEERING
www.elsevier.com/locate/ijimpeng

Modeling of simultaneous ground shock and airblast pressure on nearby structures from surface explosions

Chengqing Wu*, Hong Hao

School of Civil and Resource Engineering, The University of Western Australia, 35 Stirling Highway, Crawley WA 6009, Australia

Received 27 August 2003; accepted 1 March 2004

Abstract

A surface explosion generates both ground shock and airblast pressure on nearby structures. Although ground shock usually arrives at a structure foundation earlier than airblast pressure because of the different wave propagation velocities in geomaterials and in the air, ground shock and airblast might act on the structure simultaneously, depending on the distance between the explosion center and the structure. Even though they do not act simultaneously, ground shock will excite the structure and the structure will not respond to airblast pressure with zero initial condition. Therefore, an accurate analysis of structure response and damage to a nearby surface explosion should take both ground shock and airblast pressure into consideration. But current practice usually considers only airblast pressure. Many empirical relations are available to predict airblast pressure. Most of them, however, only predict peak pressure values. The primary objective of this study is to define simultaneous ground shock and airblast forces that can be easily applied in structural response analysis. Parametric numerical simulations of surface explosions are conducted. Empirical expressions of airblast pressure time history as a function of surface explosion charge weight, distance to structure, structure height, as well as the ground shock time history spectral density function, envelope function and duration are derived. Time lag between airblast pressure and ground shock to structure is also determined. The empirical formulae are all given in analytical forms and they can be used in structural response analysis to surface explosions.

Keywords: Simultaneous ground shock and airblast pressure; Numerical simulation; Structural response; Surface explosion; Time lag

*Corresponding author. Tel.: +61-8-938-081-82; fax: +61-8-938-010-18.
E-mail address: wu@civil.uwa.edu.au (C. Wu).

0734-743X/$ - see front matter © 2004 Elsevier Ltd. All rights reserved.
doi:10.1016/j.ijimpeng.2004.03.002

1. Introduction

Some structures need be designed against explosive loading. For example, structures in a chemical plant need be designed to withstand accidental chemical explosions. Important buildings and some lifeline infrastructures might be targets of terrorist threat and need be designed against such threats. Current practice in designing structures against surface explosive loading usually considers only the airblast pressures generated by the explosion. A surface explosion, in fact, generates both ground shock and airblast pressure on a structure. Although the ground shock reaches the structure foundation before the airblast pressure, both the ground shock and airblast might act on the structure simultaneously, depending on the distance between the explosion center and the structure. Even though they do not act on the structure simultaneously, ground shock will excite the structure and the structure will not respond to airblast pressure from rest. But little information is available for simultaneous ground shock and airblast pressure loads generated by surface explosions on structures in the literature.

The airblast pressures generated by surface explosions have received considerable attention for a long time. Many empirical formulae and empirical curves have been proposed for prediction of peak overpressure attenuation against scaled distance, pressure time history of shock wave, and shock wave reflection to structures [1–4]. These formulae can predict shock wave propagation in the air. However, certain parameters, which are essential for modeling simultaneous ground shock and airblast, such as arrival time of airblast wave to structures, are not commonly available. These available empirical relations are usually inconvenient to use since many parameters are given in empirical curves rather than in analytical equations. Often, simplified estimations have to be adopted. For example, airblast pressures are usually assumed as having a triangular or an exponential decay shape with the pressure rising phase being completely neglected. The pressure is also assumed uniformly distributed along the structural height. Such simplifications are expected to introduce errors in estimation of airblast loads on structures.

Study of blast-induced ground shock due to underground explosion has also been quite extensive in the last two decades. Both continuum and discontinuum models have been used to simulate blast-induced stress wave in rock masses [5–13]. Such models are able to give a reasonable estimation of ground motions on rock surface generated by underground explosions. In most of the previous studies, only empirical formulae for prediction of stress wave peak particle acceleration (PPA), peak particle velocity (PPV) and principal frequency (PF) were derived. Analysis of nonlinear dynamic structural response to simultaneous airblast pressure and ground shock needs more detailed ground motion properties, such as arrival time, and ground shock (stress wave) time history.

In this paper, contact explosions on rock surface are simulated by using Autodyn2D program [14]. In the numerical model, air and TNT are modeled by Euler processor with equation of state of ideal gas and Jones–Wilkens–Lee (JWL), respectively. A calibrated model for a granite mass, which includes the Hugoniot equation of state, modified Drucker–Prager strength criterion with the strain rate effect and a double scalar damage model accounting for both the compression and tension damage [15], is employed in the numerical calculations. Numerical results of the free air peak pressure attenuation against scaled distance, pressure time histories, ratio of peak reflected pressure on a rigid wall to peak free air pressure, the pressure distribution along the vertical direction are obtained and compared with other available various empirical formulae. The present

numerical results give very good predictions of airblast pressures in the free air and on a vertical rigid wall. The analytical airblast pressure time history, arrival time and rising time, which are not commonly available in existing empirical formulae and design manuals, are also derived and presented in this paper. In addition, PPA attenuation of stress wave on ground surface against scaled distance is also determined. The normalized envelope function of the stress wave time history and power spectra are derived as functions of charge weight and distance. The duration of the ground shock is obtained. They can be used to simulate stress wave time histories. The time lag between airblast pressure and ground shock is also derived as a function of the distance and charge weight. The present results allow a detailed modeling of the simultaneous airblast pressure and ground shock on structures.

2. Numerical model

A numerical model to simulate granite mass response to explosive loading, which was developed and validated against field blast tests [15], is employed in the present study. Following briefly introduces this model. It assumes that damage is generated by activation and growth of flaws and cracks due to tension and compression. Thus, a damage model with double scalars, D_t and D_c, which correspond respectively to damage measured in uniaxial tension and uniaxial compression states of rock material are used in the present study. The two scalars are defined as

$$D_t = 1 - e^{-\alpha^+ V_o(\bar{\varepsilon}^+ - \varepsilon_0^+)^{\beta^+}} \text{ and } D_c = 1 - e^{-\alpha^- V_o(\bar{\varepsilon}^- - \varepsilon_0^-)^{\beta^-}}, \tag{1}$$

where V_0 is a unit volume, α^+, α^-, β^+, and β^- are damage parameters associated with the tensile and compressive damage scalars; ε_0^+ and ε_0^- are threshold strains in uniaxial tensile and compressive state. Below the threshold strains, rock material exhibits elastic property and no damage occurs. $\bar{\varepsilon}^+$ and $\bar{\varepsilon}^-$ are equivalent tensile and compressive strains, and they are

$$\bar{\varepsilon}^+ = \sqrt{\sum_{i=1,3}(\varepsilon_i^+)^2} \text{ and } \bar{\varepsilon}^- = \sqrt{\sum_{i=1,3}(\varepsilon_i^-)^2}, \tag{2}$$

where ε_i^+ is the positive principal strain, the superscript $(+)$ means it vanishes if it is negative. ε_i^- is negative principal strain and it vanishes if it is positive.

Combining the tension and compression damage, the cumulative damage scalar D for rock material can be determined as follows:

$$D = \alpha_t D_t + \alpha_c D_c, \quad \dot{D}_t > 0, \quad \dot{D}_c > 0 \text{ and } \alpha_t + \alpha_c = 1 \tag{3}$$

where the weights α_t and α_c are defined by the following expressions:

$$\alpha_t = \sum_{i=1,3} \frac{H_i[\varepsilon_i^+(\varepsilon_i^+ + \varepsilon_i^-)]}{\tilde{\varepsilon}^2}, \quad \alpha_c = \sum_{i=1,3} \frac{H_i[\varepsilon_i^-(\varepsilon_i^+ + \varepsilon_i^-)]}{\tilde{\varepsilon}^2}, \tag{4}$$

where $\tilde{\varepsilon} = \sqrt{\sum_{i=1,3}(\varepsilon_i^+ + \varepsilon_i^-)^2}$ is the effective strain; $H_i[x] = 0$ when $x < 0$ and $H_i[x] = x$ when $x \geq 0$. It can be verified that in uniaxial tension, $\alpha_t = 1$, $\alpha_c = 0$, $D = D_t$ and vice versa in

compression. The constitutive law is then written as

$$E^* = E(1 - D_0)(1 - D), \tag{5}$$

$$G^* = G(1 - D_0)(1 - D), \tag{6}$$

where E, G and v are the undamaged Young's modulus, shear modulus and Poisson's ratio of rock material, respectively. D can be determined by Eq. (3) and D_0 is the initial damage of the rock mass. The initial damage can be estimated by comparing the in-situ P wave velocity of rock mass with laboratory sonic velocity of intact core obtained from the rock mass [16]

$$D_0 = (v_L/v_F)^2 \tag{7}$$

where v_L is in situ P wave velocity and v_F is P wave velocity in intact rock core.

The material constants of the rock mass obtained from site investigation are used in numerical simulation [15,17]. The rock mass under consideration was granite with low content of quartz and large content of feldspar, with a blocky structure. The granite is of good quality with RQD values between 75–100 and Q-value of over 10. The investigation revealed that the average P wave velocity of intact rock core is around 6000 m/s and the average in situ P wave is around 5660 m/s. Using the values, the initial damage is estimated to be 0.11. Rock tests indicated the elastic modulus of the rock material is 59.6 GPa, and unaxial compressive and tensile strength: 226.2 and 12.6 MPa, the threshold strains ε_0^+ and ε_0^-: 2.1×10^{-4} and 3.8×10^{-3}, respectively. The material constants α_i and β_i are $\alpha^+ = 6.89 \times 10^{10}$, $\alpha^- = 1.19 \times 10^7$, $\beta^+ = 2$ and $\beta^- = 2$.

Besides the above damage model, a modified Drucker–Prager strength criterion and the Hugoniot equation of state (EOS) are also used in the numerical model [15]. The Hugoniot EOS for the rock material can be expressed as

$$p = (K_1\mu + K_2\mu^2 + K_3\mu^3)(1 - D_0)(1 - D), \tag{8}$$

where μ is the compression factor; K_1, K_2, and K_3 are material constants and they are 5.76×10^{10}, 9.91×10^{10} and 6.39×10^{10} Pa, respectively. The modified Drucker-prager strength criterion can be expressed as

$$F = \sqrt{J_2} - \alpha I - k', \tag{9}$$

where J_2 is the second invariant of the stress deviator and I is the first invariant of the stress tensor given by $J_2 = 0.5 s_{ij} s_{ij}$; $I = (\sigma_1 + \sigma_2 + \sigma_3)$, $k' = k(1 - D_0)(1 - D)[A \log(\dot{\sigma}_{cd}/\dot{\sigma}_c) + \sigma_c]/\sigma_c$ in which σ_{cd} is the dynamic uniaxial compressive strength (MPa), $\dot{\sigma}_{cd}$ is the dynamic loading rate, σ_c is the uniaxial compressive strength at the quasi-static loading rate $\dot{\sigma}_c$, α and k are material constants and $A = 11.9$ is a material parameter.

The above models were programmed and linked to Autodyn2D [14] as its user provided subroutines. In the numerical model, air and TNT are simulated by Euler processor and are presumed to have equation of state of ideal gas and of JWL, respectively. The standard constants of air and TNT from Autodyn2D material library are utilized in the numerical model, including air mass density $\rho = 1.225\,\mathrm{kg/m^3}$; air initial internal energy $E_n = 2.068 \times 10^5\,\mathrm{kJ/kg}$; ideal gas constant $l = 1.4$. More detailed description of the models and their implementation can be found in a previous paper [15].

The above numerical model is used to simulate airblast pressures and ground shock from surface explosions in the present study. It should be noted that site properties will actually affect

stress wave propagation. It will not be possible to define a site property that represents all the different site conditions. Current results using granite is valid for sites with similar conditions. For a site with different ground properties, different results might be obtained.

3. Overpressure in the free air from surface explosions

Using the numerical model, shock wave propagation in the air from explosions on rock surface is simulated. Fig. 1 shows the configuration of the simulation model. The whole domain, including rock and air, is assumed to be Z-axis symmetric. As shown, the explosive (TNT) in a spherical shape is placed on the surface of the rock mass. The TNT charge weight used in simulations is, respectively, 300, 500, 1000, 1500, 2000, and 10 000 kg. The pressure time histories in each case in the air at the target points directly above the ground surface as indicated in Fig. 1 are recorded. Fig. 2 shows simulated ground shock and airblast pressure time histories from 1t surface explosion. As shown, when the distance from a structure to explosive center is 30 m, simultaneous ground shock and airblast pressure do not act on the structure simultaneously. When the distance from a structure to explosive center is 20 m, there is partially overlap for ground shock and airblast pressure on the structure. When the distance is 10 m, ground shock and airblast pressure act on the structure at almost the same time. Fig. 3 shows typical simulated pressure time histories in the air. The shock wave is characterized by a sudden pressure rise to the peak value at the shock front, and followed by a quasi-exponential decrease back to ambient value and then a negative phase. The parameters needed to model the shock wave time history include: the shock wave front arrival time T_a, the rising time from arrival time to the peak value T_r, peak pressure p_{so}, the decreasing time from peak to the ambient pressure T_d.

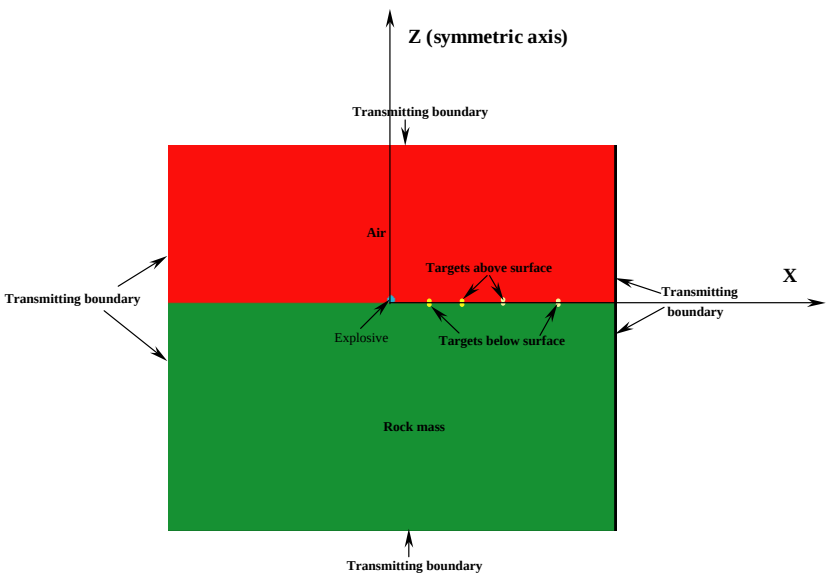

Fig. 1. Configuration of numerical model of surface.

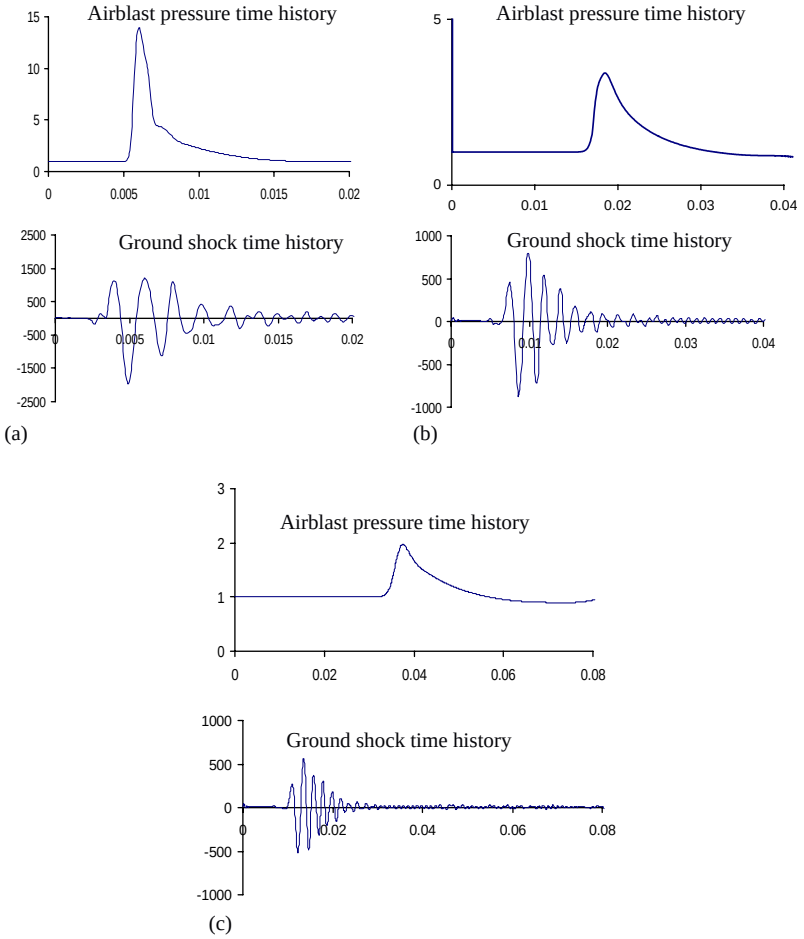

Fig. 2. Simulated ground shock and airblast pressure time histories from 1t surface explosion. (a) 10 m from charge center. (b) 20 m from charge center. (c) 30 m from charge center.

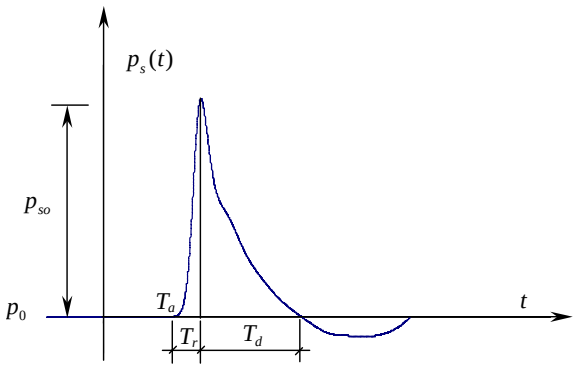

Fig. 3. Typical free-air pressure time history.

Using the simulated pressure time histories, the peak values at each point in the air can be determined. Based on these data, empirical attenuation relations for peak air pressure at a hemispherical front were derived as

$$p_{so} = 1.059\left(\frac{R}{Q^{1/3}}\right)^{-2.56} - 0.051, \quad 0.1 \le R/Q^{1/3} \le 1 \quad \text{(MPa)}, \tag{10}$$

$$p_{so} = 1.008\left(\frac{R}{Q^{1/3}}\right)^{-2.01}, \quad 10 \ge R/Q^{1/3} > 1 \quad \text{(MPa)}, \tag{11}$$

where R is the distance in meters measured from the charge center and Q is the TNT charge weight in kilograms. Fig. 4 shows the numerically simulated values and their best-fitted curve.

Many empirical formulae for predicting peak pressures in the air are available in the literature. Most of them were obtained from field blast tests [1,3,18]. Brode's empirical formulae for peak pressure at shock wave front in an unlimited atmosphere are in the form of [18]

$$p_{so} = 0.67\left(\frac{R}{Q^{1/3}}\right)^{-3} + 0.1, \quad p_{so} > 1 \quad \text{(MPa)}, \tag{12}$$

$$p_{so} = 0.098\left(\frac{R}{Q^{1/3}}\right)^{-1} + 0.1465\left(\frac{R}{Q^{1/3}}\right)^{-2} + 0.585\left(\frac{R}{Q^{1/3}}\right)^{-3} - 0.0019, \quad 0.01 \le p_{so} \le 1 \quad \text{(MPa)}, \tag{13}$$

Henrych's empirical formulae in an unlimited atmosphere are [1]:

$$p_{so} = 1.4072\left(\frac{R}{Q^{1/3}}\right)^{-1} + 0.554\left(\frac{R}{Q^{1/3}}\right)^{-2} - 0.0357\left(\frac{R}{Q^{1/3}}\right)^{-3} + 0.00006.25\left(\frac{R}{Q}\right)^{-4}, \quad 0.1 \le R/Q^{1/3} < 0.3 \quad \text{(MPa)}, \tag{14}$$

$$p_{so} = 0.619\left(\frac{R}{Q^{1/3}}\right)^{-1} - 0.033\left(\frac{R}{Q^{1/3}}\right)^{-2} + 0.213\left(\frac{R}{Q^{1/3}}\right)^{-3}, \quad 0.3 \le R/Q^{1/3} \le 1 \quad \text{(MPa)}, \tag{15}$$

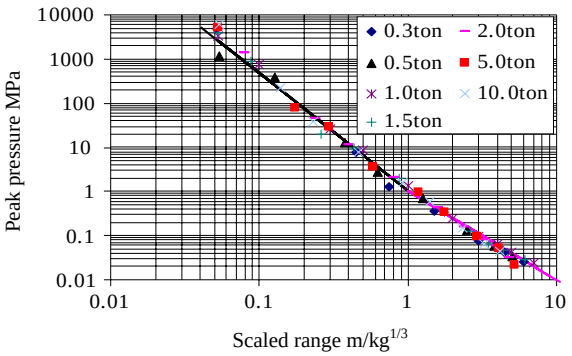

Fig. 4. Peak pressure attenuation relations corresponding to different charge weights in the free air along the horizontal direction.

$$p_{so} = 0.066\left(\frac{R}{Q^{1/3}}\right)^{-1} + 0.405\left(\frac{R}{Q^{1/3}}\right)^{-2} + 0.329\left(\frac{R}{Q^{1/3}}\right)^{-3}, \quad 1 \le R/Q^{1/3} \le 10 \quad \text{(MPa)}. \tag{16}$$

It should be noted that for predicting peak pressure of contact explosions from Eqs. (13)–(16), charge weight $2Q$ must be substituted for Q. The design manual TM-5 [3] also gives some curves obtained from field blast tests for prediction of peak pressures in the free air. Fig. 5 shows the comparisons of the peak pressure in the air predicted by the present functions and by other empirical relations. As shown, at scaled distance $R/W^{1/3}$ larger than 1.0, all the relations give very similar predictions. When $R/W^{1/3}$ is between 0.3 and 1.0, the numerical results still agree well with Henrych's and TM-5's experimental data, but quite different with Brode's. When $R/W^{1/3}$ is less than 0.3, the numerical data deviate from all the three experimental data. The data from the three empirical formulae also differ significantly when $R/W^{1/3}$ is small. This is probably because it is very difficult to measure accurately the airblast pressure at small scaled distance, either those derived from explosion tests or from numerical simulation.

The shock wave front arrival time T_a, which is usually not included in the previous studies, is estimated here. Fig. 6 shows the arrival time of shock wave front for different charge weights. As shown, at the same-scaled distance, the larger the charge weight is, the longer the arrival time is. The best-fitted function of the arrival time in terms of distance and charge weights is

$$T_a = 0.34R^{1.4}Q^{-0.2}/c_a \quad (s), \tag{17}$$

where C_a is the sound speed in the air, which is 340 m/s.

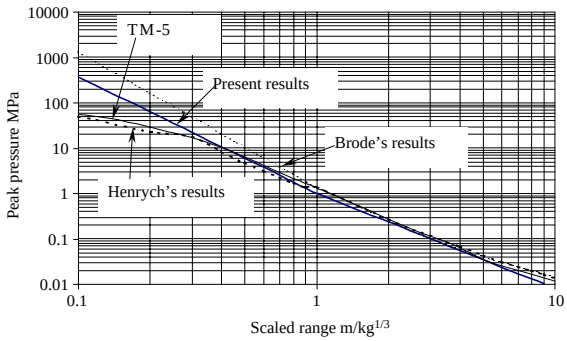

Fig. 5. Comparison of peak pressure attenuation against scaled distance.

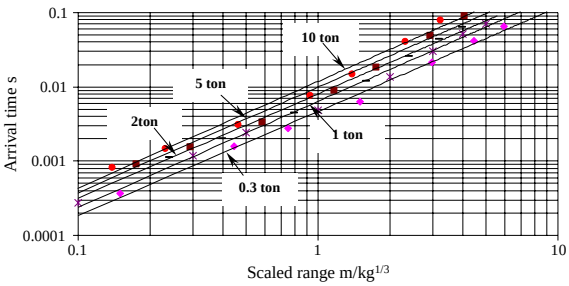

Fig. 6. Arrival time of shock wave front for different charge TNT weights.

Another parameter is the rising time for pressure to rise suddenly from zero to peak value. In most previous studies, this phase in the pressure time history is not modeled because the rising time is very short. The pressure time history is usually assumed starting from the peak value and decreases either exponentially or linearly. For a more accurate modeling of the airblast pressure time history, this phase is included in this study. The pressure is assumed to increase linearly from zero to its peak value with a rising time T_r. Fig. 7 shows the rising time at different scaled distances. It is noteworthy that the rising time is proportional to the scaled distance regardless of charge weights. Based on the simulated data, the best-fitted relation is

$$T_r = 0.0019(R/Q^{1/3})^{1.30} \quad \text{(s)}, \tag{18}$$

The decreasing time for the pressure time history to decrease from its peak value to the ambient pressure is another parameter for modeling the pressure time history. Fig. 8 shows the decreasing time of the simulated pressure time history. It shows that at the same scaled distance, the heavier the charge weight, the longer the decreasing time. Using the simulated data, an empirical attenuation relation for the decreasing time is derived as

$$T_d = 0.0005(R/Q^{1/3})^{0.72}Q^{0.4} = 0.0005R^{0.72}Q^{0.16} \quad \text{(s)}, \tag{19}$$

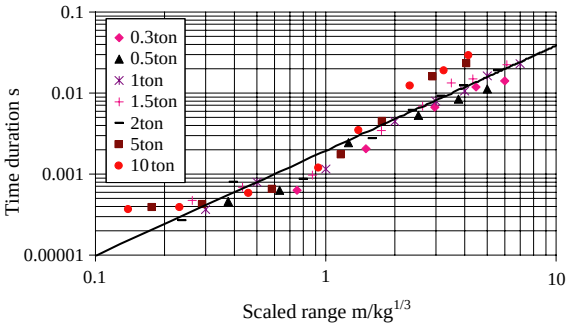

Fig. 7. Duration for the pressure to increase from zero to peak value.

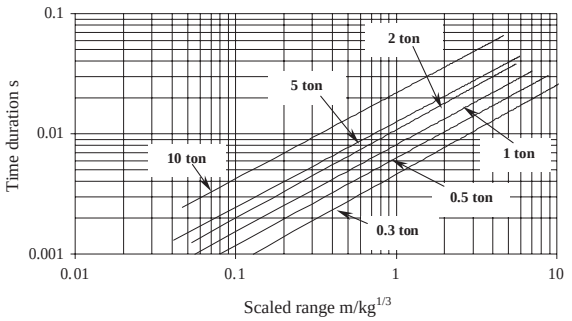

Fig. 8. Duration for the pressure to decrease from peak value to ambient pressure.

Combining Eqs. (18) and (19), the duration of the positive pressure of the airblast pressure wave can be written as

$$T_+ = T_\mathrm{r} + T_\mathrm{d}. \tag{20}$$

The duration of the positive pressure phase of the shock wave can also be estimated by other empirical formulae. Henrych [1] used the experimental data in TNT-charge explosions and derived the following formula:

$$T_+ = 10^{-3}[0.107 + 0.444(R/Q^{1/3}) + 0.264(R/Q^{1/3})^2 - 0.129(R/Q^{1/3})^3 + 0.0335(R/Q^{1/3})^4]Q^{1/3} \quad 0.05 \le R/Q^{1/3} \le 3 \quad \text{(s)}. \tag{21}$$

The design manual TM-5 [3] also gives charts to predict T_+. Fig. 9 shows the comparison of the positive pressure duration estimated by different empirical relations. As shown, the present result is very close to Henrych's, but does not compare well with TM-5's. The largest error is about two times. This difference can be partially attributed to reading error from the graphs given in the TM-5. Nevertheless, the above comparison indicates that the present empirical relation gives reasonable prediction of the positive pressure duration.

In the present study, the airblast pressure time history is simplified to two parts (see Fig. 3): a sudden linear pressure rise to the peak value, then followed by an exponential decay. The linear part for the pressure rising from zero to its peak value is

$$p_\mathrm{s}(t) = p_\mathrm{so}\left(\frac{t}{T_\mathrm{r}}\right) = 526.3tp_\mathrm{so}(R/Q^{1/3})^{-1.30}, \quad 0 \le t \le T_\mathrm{r} \tag{22}$$

The exponential decay phase is modeled by the same function used in most of the previous studies [1,2,19]. It is expressed as

$$p_\mathrm{s}(t) = p_\mathrm{so}\left(1 - \frac{t - T_\mathrm{r}}{T_d}\right)\exp\left(-\frac{a(t - T_r)}{T_d}\right), \quad T_r \le t, \tag{23}$$

where a is a constant controlling the rate of decay. The best-fitted functions for a value from the simulated pressure time histories are

$$a = \begin{cases} 3.02p_\mathrm{so}^{0.38} + 6.85p_\mathrm{so}^{0.79}\exp\left(-4.55\dfrac{t - T_\mathrm{r}}{T_\mathrm{d}}\right), & T_r \le t \le T_+, \\ 1.96p_\mathrm{so}^{0.25} + 0.176p_\mathrm{so}\exp\left(-0.73p_\mathrm{so}^{-0.49}\dfrac{t - T_+}{T_\mathrm{d}}\right), & T_+ < t, \end{cases} \tag{24}$$

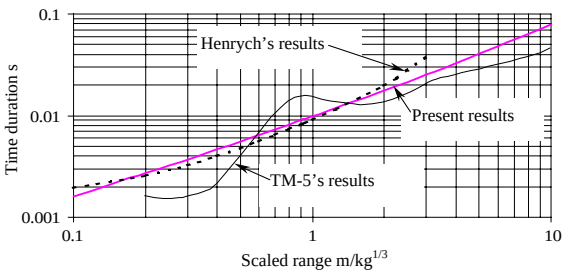

Fig. 9. Estimated duration of the positive pressure with a charge weight of 1000 kg.

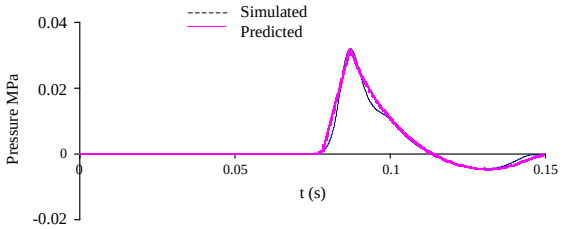

Fig. 10. The simulated and predicted airblast pressure time histories at 50m from charge center when charge weight is 1000 kg.

for $p_{so} \leq 1$ MPa, and

$$a = \begin{cases} 1.62p_{so}^{0.3} + 5.13p_{so}^{0.28}\exp\left(-1.05p_{so}^{0.37}\dfrac{t-T_r}{T_d}\right), & T_r \leq t \leq T_+, \\ 0.74p_{so}^{0.17} + 2.71p_{so}^{0.28}\exp\left(-0.26p_{so}^{0.33}\dfrac{t-T_r}{T_d}\right), & T_+ < t, \end{cases} \tag{25}$$

for 1 MPa $\leq p_{so} \leq 100$ MPa. It should be noted that p_{so} in the above formulae is in MPa.

There are also other empirical formulae to estimate constant a. For example, Henrych suggested: $a = 0.5 + 10p_{so}$ for $p_{so} \leq 0.1$ MPa and $a = 0.5 + 10p_{so}[1.1 - (0.13 + 2p_{so})(t/T_+)]$ for $0.1 \leq p_{so} \leq 0.3$ MPa [1], where p_{so} in the above formulae is also in MPa. However, it is found that Eqs. (24) and (25) result in better predictions of the simulated pressure time histories. Moreover, the result by Henrych's is only valid for the prediction of the positive phase of the pressure time history, and is valid for a lower peak pressure range as compared to Eqs. (24) and (25). Fig. 10 shows the simulated and the predicted airblast pressure time histories using the relations derived above at a distance of 50 m from the charge center and a charge weight of 1000 kg. As shown, the predicted pressure time history agrees very well with the simulated data.

4. Shock wave reflection from a rigid wall

In order to study the influence of simultaneous ground shock and airblast pressure on structures, the pressures on front surface of a structure should be determined. Fig. 11 shows the configuration of numerical simulation of surface explosions with a rigid wall at a distance R from the charge center. Z-axis symmetry is assumed for the numerical model. Targets are placed along the front surface of the wall and in the free air symmetric to the charge center to record the pressure time histories and to investigate their differences. It is found that the reflected pressure time histories have the same shape as those in the free air. Other researchers also made similar observations in the previous studies [1,3]. The ratio of the peak reflected pressure to the peak free air pressure is calculated. Fig. 12 shows the ratio of horizontal (normal to the wall) peak reflected pressure to peak air pressure. It shows that the ratio increases with the peak free air pressure. The best-fitted relation of the peak reflected pressure to the peak free air pressure is

$$p_{ro} = 2.85(p_{so})^{1.206}, \quad p_{so} \leq 50 \quad \text{(MPa)}, \tag{26}$$

where P_{ro} is the normal peak reflected pressure at the bottom of the rigid wall. The reflected pressure along the height of the wall will be discussed later.

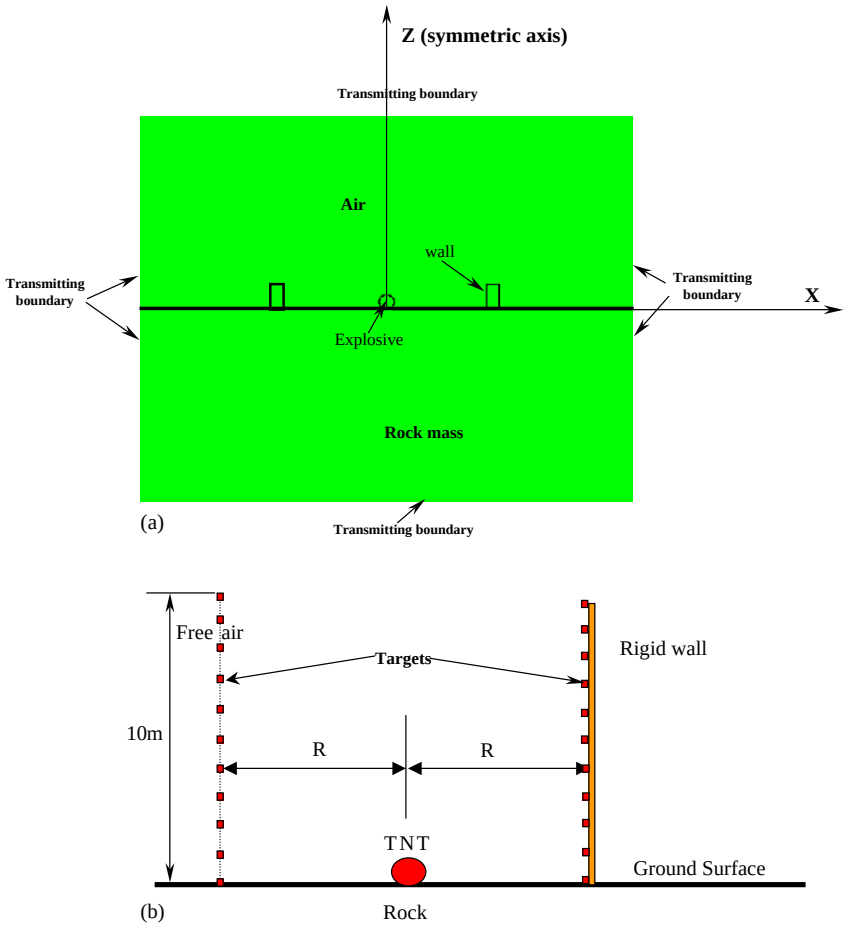

Fig. 11. Configuration of numerical model of surface explosion with wall reflection. (a) Numerical model set up. (b) Targets on rigid wall and in the free air to record pressure time history. 11 targets on each side at 1 m increment.

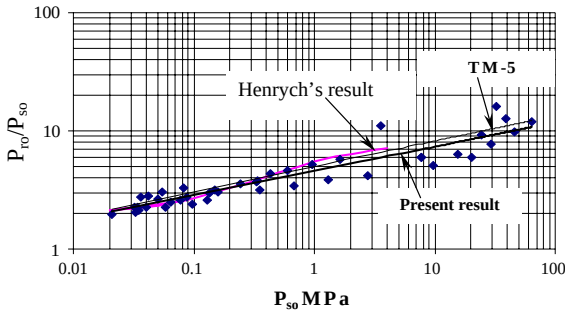

Fig. 12. Ratios of horizontal peak reflected pressure to the peak free air pressure.

The present result is also compared with those obtained by other researchers. Henrych derived an empirical relation as [1]

$$p_{ro} = \frac{8p_{so}^2 + 14p_{so}}{p_{so} + 7.2}, \quad p_{so} \le 4 \quad \text{(MPa)}. \tag{27}$$

The design manual TM-5 [3] also gives curves to predict the peak reflected pressure from the peak free air pressure. A comparison of the empirical relations is shown in Fig. 12. It shows that when the peak free air pressure is less than 0.2 MPa, Henrych's formula matches very well with the present result; but when the peak pressure is higher than that value, the difference becomes bigger. It also shows that the present result agrees well with that predicted by TM-5.

5. Pressure distribution along the rigid wall

The pressure distribution along the rigid wall is also investigated to determine the variations of the airblast forces along the structure height. Fig. 13 shows the reflected pressure along the rigid wall normalized by the reflected pressure at the bottom of the wall. It shows that the normalized reflected pressure decreases with the wall height. The nearer is the wall to the charge center, the steeper is the pressure descending curve. This indicates that the uniform distribution assumption of the airblast loads along the structural height, commonly adopted in most design analysis, might introduce significant errors if the explosive center is very close to the structure. The descending curve is in the form of

$$p_r(h) = p_{ro}(1 - bh^2), \quad p_{ro} \le 10 \quad \text{(MPa)}, \tag{28}$$

where h is the height of the wall in meters and b is a constant which depends on pressure p_{ro}. Based on the numerical data, the relationship between b and p_{ro} is derived as

$$b = 0.0006p_{ro}^{0.46}, \quad p_{ro} \le 10 \quad \text{(MPa)}, \tag{29}$$

where p_{ro} is estimated by Eq. (26). Eq. (28) can be rewritten as

$$p_r(h) = p_{ro}(1 - 0.0006p_{ro}^{0.46}h^2), \quad p_{ro} \le 10 \quad \text{(MPa)}. \tag{30}$$

With Eq. (30), the pressure distribution along the structural height can be estimated.

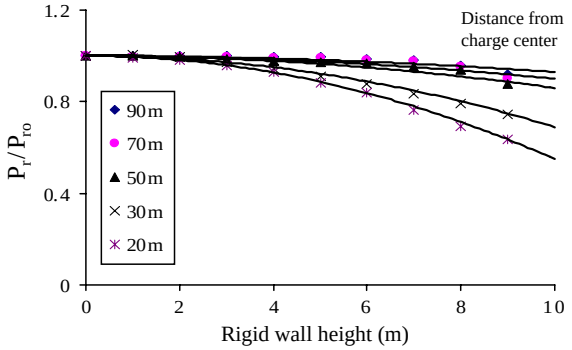

Fig. 13. The reflected pressure distribution along the rigid wall normalized by the reflected pressure at the bottom of the wall.

6. Ground shock wave from surface explosions

When analyzing structural response under simultaneous ground shock and airblast force, it is also necessary to know the expected blast-induced ground motion time history. A ground motion time history is completely defined by its peak value, duration, shape function, and power spectrum. In addition, the arrival time of ground motion is also needed for structure response analysis to simultaneous airblast pressure and ground shock. The numerically simulated ground motion time histories on rock surface are used to derive the above parameters in this study.

Fig. 14 shows a typical simulated acceleration time histories on rock surface at a distance of 10 m from the charge center with a 2-ton charge weight. It shows that acceleration in the horizontal direction is much larger than that in the vertical direction. The plot shown in Fig. 15 gives peak ground acceleration attenuation with the scaled distance on rock surface corresponding to different charge weights. It shows that the larger the charge weights, the higher the PPA at the same-scaled distance and vice versa. The observation is opposite to those obtained from underground explosion reported in a previous study [11]. In the later study, it was found that the larger is the charge weight, the lower is the PPA at the same scaled distance in the rock mass. This is because the dominant frequency of the stress wave propagating inside the rock mass generated from an underground explosion could be more than 10,000 Hz. A larger charge weight results in more severe damage and a larger damaged zone in the rock mass around the charge center as compared to a small charge weight. Damage in the rock mass causes rapid attenuation of high frequency stress wave. On the other hand, the dominant frequency of stress wave propagating along the rock surface generated from a surface explosion is in an order of 100–1000 Hz. Damage of the rock mass does not filter out the stress waves at such frequencies, rather, it seems amplifying

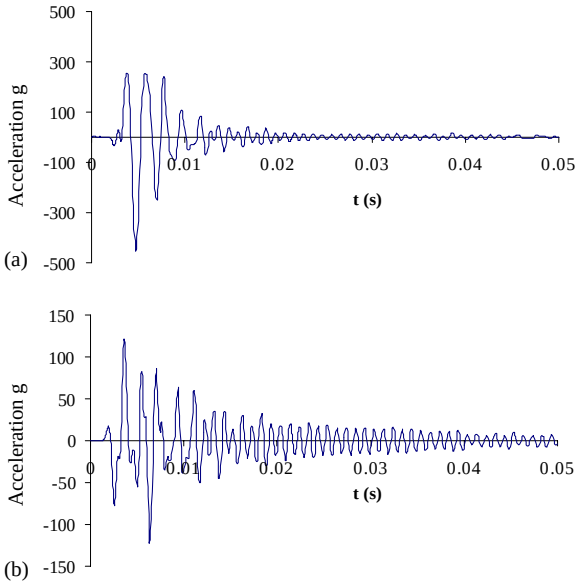

Fig. 14. The simulated acceleration time histories on rock surface at a distance of 10 m from charge center with a charge weight of 2 ton. (a) Horizontal direction. (b) Vertical direction.

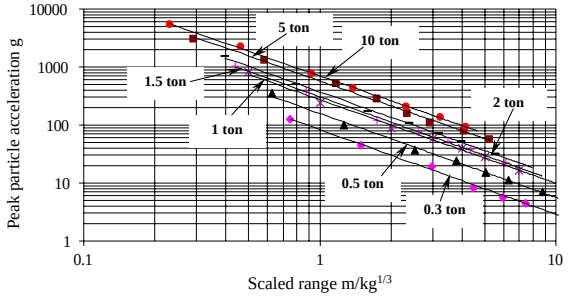

Fig. 15. The simulated PPA attenuation on rock surface at different scaled distance under different charge weights.

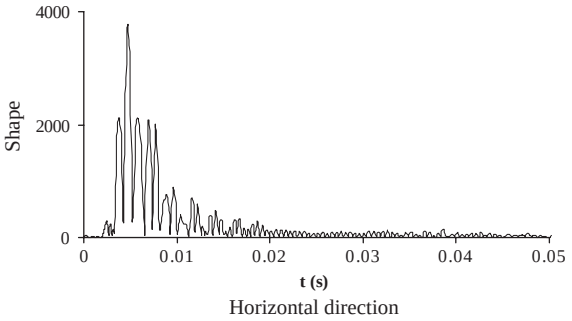

Fig. 16. The envelope function for simulated acceleration time histories on rock surface at 10 m from the charge center with a charge weight of 2 ton.

the stress wave. More studies, both parametric analysis and experimental investigation, however, are needed to confirm this argument.

The best-fitted PPA of surface ground motion as a function of charge weight and distance is

$$\mathrm{PPA} = 3.979R^{-1.45}Q^{1.07} \quad (\mathrm{g})\,. \tag{31}$$

Arrival time of ground motions is needed in modeling the simultaneous ground shock and airblast forces on structures. From the simulated data, the arrival time at a point on ground surface with a distance R from the charge center can be simply estimated by

$$t_a = 0.91R^{1.03}Q^{-0.02}/c_s \quad (\mathrm{s}) \tag{32}$$

where c_s is the P wave velocity of the granite mass.

The shape function is used to characterize seismic ground vibration nonstationarity in the time domain in earthquake engineering. In the present study, it is also used to characterize blast-induced surface vibrations. Fig. 16 shows the shape function of a simulated acceleration time history in the horizontal direction on rock surface at a distance of 10 m from charge center when charge weight is 2 ton. It is obtained by the Hilbert transform [20]. It indicates that the envelope of the blast motions can be best modeled by the exponential type shape function [21]. It has the form of

$$\xi(t) = \begin{cases} 0, & t \le 0, \\ mte^{-nt^2}, & t > 0, \end{cases} \tag{33}$$

where m and n are parameters related to ground motion nonstationarity, e is the base of the natural logarithm. The two parameters m and n are determined by t_p, at which $\xi(t)$ reaches its maximum value of unity. t_p is the duration for ground shock to reach its peak value from t_a. It has the form

$$t_p = \sqrt{1/2n}, \tag{34}$$

$$m = \sqrt{2ne}. \tag{35}$$

From the simulated data, the empirical relation for estimating the time instant t_p is derived as

$$t_p = 5.1 \times 10^{-4} Q^{0.27} (R/Q^{1/3})^{0.81} = 5.1 \times 10^{-4} R^{0.81} \quad \text{(s)}. \tag{36}$$

As shown, t_p depends on distance R only.

Duration of shock wave is also a very important parameter that affects the structural response. In this study, shock wave duration t_d is defined as

$$t_d = t - t_a, \tag{37}$$

where t_d is determined when error of the equivalent kinetic energy of the ground motion is less than 5% if the remaining part of the motion is cut off. In other words, it is determined by, $(E_t - E_{t-0.005})/E_t \leq 0.05$, and $E_t = \left(\frac{1}{2}\right) \int_0^t v^2 \, dt$, in which v is the ground motion velocity time history (see Fig. 17). From the simulated data, it is found that

$$t_d = 0.0045 R^{0.45} \quad \text{(s)}. \tag{38}$$

Frequency contents of stress wave play an important role in determining the response of a structure. In the previous study, principal frequency of an acceleration time history was defined as [11]

$$\text{PF} = \frac{F_1 + F_2}{2}, \tag{39}$$

where F_1 and F_2 are determined by the intersection points of a horizontal line at $F_{max}/2$ on the Fourier spectrum of the acceleration time history, in which F_{max} is the peak value of the Fourier spectrum, as shown in Fig. 18. PF alone, however, is not enough to characterize the frequency contents of blast-induced stress wave. Accurate estimation of frequency contents should include the power spectrum function. By comparison, it is found that the power spectrum of blast-induced ground motions can also be represented by a Tajimi–Kanai function [22], which has been widely

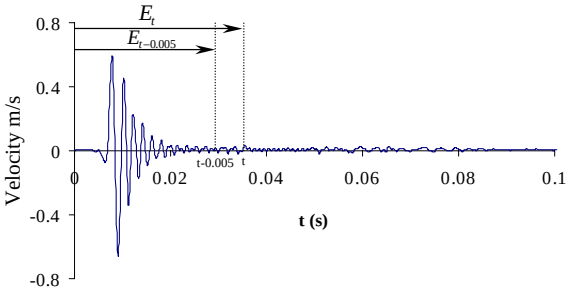

Fig. 17. Definition of stress wave duration.

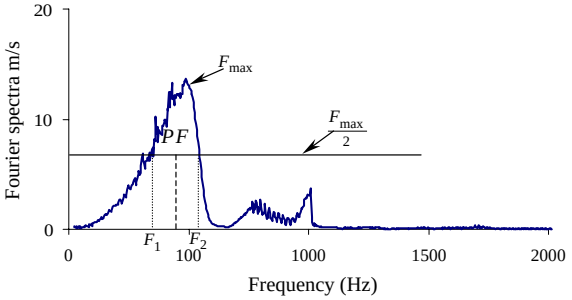

Fig. 18. Definition of principal frequency (PF).

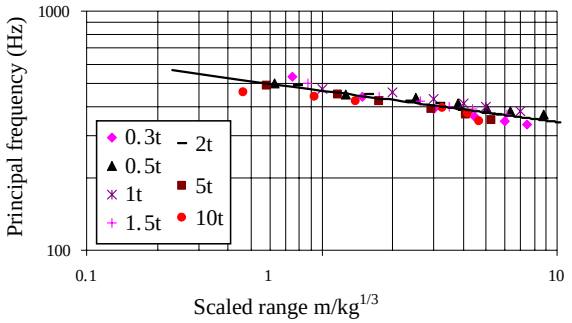

Fig. 19. Principal frequency of shock wave on rock surface at different scaled distances under different charge weights.

used in earthquake engineering. The power spectrum is

$$S(f) = \frac{1 + 4\varsigma_g^2 f^2/\mathrm{PF}^2}{\left(1 - f^2/\mathrm{PF}^2\right)^2 + 4\varsigma_g^2 f^2/\mathrm{PF}^2} S_o, \tag{40}$$

where S_o is the amplitude of power spectrum of a white noise or a scaling factor of the spectrum, PF is the principal frequency and ζ_g is a parameter governing the power spectral shape. Fig. 19 shows the plot of the principal frequency (PF) at different scaled distances and charge weights. The empirical relation is derived as

$$\mathrm{PF} = 465.62(R/Q^{1/3})^{-0.13}, \quad 0.3 \le R/Q^{1/3} \le 10 \quad (\mathrm{Hz}). \tag{41}$$

A constant ζ_g value of 0.16 is found for all the simulated time histories. The scaling factor of the spectrum is

$$S_o = 1.49 \times 10^{-4} R^{-2.18} Q^{2.89}, \quad (\mathrm{m}^2/\mathrm{s}^3). \tag{42}$$

Fig. 20 illustrates the predicted and simulated power spectrum of an acceleration time history at 21 m from charge center when charge weight is 1 ton. As shown the predicted result agrees well with the simulated data.

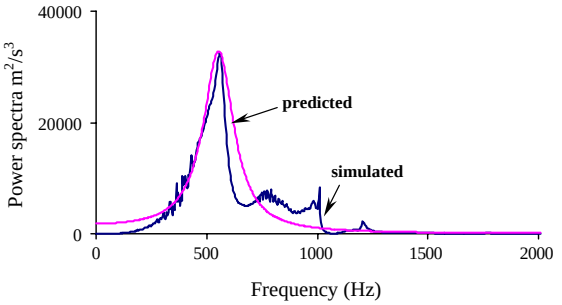

Fig. 20. Predicted and simulated of power spectrum of an acceleration time history at 5 m from the charge center with the charge weight of 1 ton.

Using the above empirical formulae for PPA, the envelope function, duration, and power spectrum function, the expected blast-induced ground motions can be simulated. It should be noted that these formulae are valid in the range of the scaled distance 0.3–10.

7. Time lag between ground shock and airblast pressure arrival at structures

From the above empirical relation (17) and (32), the time lag between the ground shock and airblast pressure reaching to the structure can be estimated by

$$T_{\text{lag}} = T_{\text{a}} - t_{\text{a}} = 0.34R^{1.4}Q^{-0.2}/c_{\text{a}} - 0.91R^{1.02}Q^{-0.02}/c_{\text{s}} \quad \text{(s)}. \tag{43}$$

It should be noted that the time lag is not only related to distance from charge center and charge weight, but also to wave propagation velocity in the air and at the site. At the same distance, the larger the charge weight, the shorter the time lag.

8. Conclusions

Numerical models including both free air and rock material properties were programmed and linked to Autodyn2D as its user provided subroutines. They were employed to simulate ground shock and airblast pressures generated from surface explosions. Parameters for predicting the pressure time histories in the free air, ratio of peak reflected pressure on a rigid wall to peak free air pressure, have been presented as a function of the scaled distance and peak pressure. They were found in good agreement with the previous studies. The analytical airblast pressure time history, arrival time and rising time were derived and the pressure distribution along the structural height is determined. Parameters for predicting blast-induced ground motions such as the PPA, arrival time, duration, and the power spectrum as well as the envelope function of ground motion were obtained. The time lag between airblast pressure and ground shock arrival time at the structure was also derived. These empirical formulae can be used for more accurate estimation of explosive loads in modeling response and damage of structures to surface explosions.

References

[1] Henrych J. The dynamics of explosion and its use. Amsterdam: Elsevier; 1979.
[2] Baker WE, Cox PA, Westine PS, Kulesz JJ, Strehlow RA. Explosion hazards and evaluation. Amsterdam: Elsevier; 1983.
[3] Technical Manual (TM-5-855-1). Fundamentals of protective design for conventional weapons. Headquarters, Department of the Army, Washington, DC, 1986.
[4] Bulson PS. Explosive loading of engineering structures. Macmillan Publishers New Zealand Ltd., E&FN SPON, An Imprint of Chapman & Hall, 1997.
[5] Grady DE, Kipp ME. Continuum modelling of explosive fracture in oil shale. Int J Rock Mech Min Sci Geomech Abstr 1980;17:147–57.
[6] Yang R, Bawden WF, Katsabanis PD. A new constitutive model for blast damage. Int J Rock Meth Min Sci Geomech Abstr 1996;33:245–54.
[7] Liu L, Katsabanis PD. Development of a continuum damage model for blasting analysis. Int J Rock Mech Min Sci 1997;34:217–31.
[8] Chen SG, Zhao J. A Study on UDEC modelling of blast wave propagation in jointed rock mass. Int J Rock Mech Min Sci 1998;35:93–9.
[9] Hao H, Wu C, Seah CC. Numerical analysis of blasting-induced stress wave in anisotropic rock mass with continuum damage models. Part II: stochastic approach. Rock Mech Rock Eng 2002;35(2):95–108.
[10] Hao H, Wu C, Zhou YX. Numerical analysis of blasting-induced stress wave in anisotropic rock mass with continuum damage models. Part I: equivalent material approach. Rock Mech Rock Eng 2002;35(2):79–94.
[11] Hao H, Wu C. Scaled-distance relationships for chamber blast accidents in underground storage of explosives. Fragblast-Int J Blast Fragmentation 2001;5:57–90.
[12] Wu C, Hao H, Lu Y, Zhou YX. Characteristics of wave recorded in small scale field blast tests in a layered rock-soil medium. Geotechnique 2003;53(6):587–99.
[13] Wu C, Lu Y, Hao H, Lim WY, Zhou YX, Seah CC. Characterisation of underground blast-induced ground motions from large-scale field tests. Shock Waves, An Int J Shock Waves, Detonations Explosions 2003;13(3): 237–52.
[14] Century Dynamics. AUTODYN user manual. Revision 3.0. Century Dynamics, Inc.; 1997.
[15] Wu C, Lu Y, Hao H. Numerical prediction of blast-induced stress wave from large-scale underground explosion. Int J Numex Anal Methods Geom 2004;28(1):93–109.
[16] Wu C, Hao H, Zhou YX. Fuzzy-random probabilistic analysis of rock mass responses to explosive loads. J Comput Geotech 1999;25(4):205–25.
[17] Hanson H. Large scale tests in Alvdalen—test no. 1, 2, and 3. Technical reports to Defence Science and Technology Agency, Singapore, 2001.
[18] Brode HL. Blast wave from a spherical charge. Phys Fluids 1959;2:217.
[19] Smith PD, Hetherington JG. Blast and ballistic loading of structures. Great Britain: Butterworth-Heinemann Ltd.; 1994.
[20] Kanasewich ER. Time sequence analysis in geophysics. Edmonton, Alberta, Canada: The University of Alberta Press; 1981.
[21] Bogdanoff JL. Response of a simple structure to random earthquake type disturbance. Bull Seismol Soc Am 1960;51:293–310.
[22] Tajimi H. A statistical method of determining the maximum response of a building structure during an earthquake. Proc 2WCEE Tokyo 1960;2:781–97.